Journal of Sound and Vibration (1987) **117**(1), 115–130

MODAL COUPLING EFFECTS IN THE FREE VIBRATION OF ELASTICALLY INTERCONNECTED BEAMS

A. JOSHI AND A. R. UPADHYA

Structures Division, National Aeronautical Laboratory, Bangalore 560 017, *India*

(*Received* 28 *August* 1986, *and in revised form* 25 *October* 1986)

The problem of free vibration of a uniform beam elastically interconnected to a cantilevered beam, representing an idealized launch vehicle aeroelastic model in a wind tunnel, is studied. With elementary beam theory modelling, numerical results are obtained for the frequencies, mode shapes and the generalized modal mass of this elastically coupled system, for a range of values of the spring constants and cantilevered beam stiffness and inertia values. The study shows that when the linear springs are supported at the nodal points corresponding to the first free-free beam mode, the modal interaction comes primarily from the rotational spring stiffness. The effect of the linear spring stiffness on the higher model modes is also found to be marginal. However, the rotational stiffness has a significant effect on all the predominantly model modes as it couples the model deformations and the support rod deformations. The study also shows that though the variations in the stiffness or the inertia values of the cantilever beam affect only the predominantly cantilever modes, these variations become important because of the fact that the cantilevered support rod frequencies may come close to, or even cross over, the predominantly model mode frequencies. The results also bring out the fact that shifting of the support points away from the first mode nodal points has a maximum effect only on the first model mode.

1. INTRODUCTION

Many spacecraft such as rockets, launch vehicles, missiles, etc., are designed as slender cylindrical structures in order to achieve optimum flight performance. However, these structures generally have low flexural vibration frequencies and therefore are prone to transverse dynamic excitation arising from either unsteady flow around the spacecraft or from atmospheric turbulence or gusts. This phenomenon is commonly known as buffeting. The buffeting response of a spacecraft subjected to the unsteady pressure fluctuations, if significant, may not only induce significant dynamic stress levels but may also significantly alter the flight path. Therefore, it becomes necessary to quantify the buffet response of a spacecraft structure at the design stage itself.

Determination of the buffet response of a slender cylindrical body involves understanding the structural properties as well as the unsteady aerodynamic behaviour of the spacecraft. There have been very few theoretical studies to predict the buffet response of a spacecraft [1, 2], mainly because of the fact that the simplified aerodynamic models are generally inadequate in representing the complex nature of the true airflow pattern around the oscillating complex spacecraft configurations. Therefore, the study of the buffet response of spacecraft has largely remained in the realm of experimental testing where an appropriately scaled model of the spacecraft is subjected to airflow inside a wind tunnel [3–5]. The design of these scaled buffet models is dependent on the similarity conditions which specify that the reduced frequency parameter should be the same for both the prototype and the scaled model. This constraint can be satisfied if the natural

0022-460X/87/160115+16 $03.00/0

frequencies and the generalized modal masses of the model are appropriately scaled. Experimental studies on the models so designed have proved very useful in assessing the buffet response of a full scale structure prior to its launching. However, in all these studies the free-free boundary condition simulation poses difficulties and is also a potential source of error contributing to both the frequency and the generalized modal mass of the designed model. This is because one necessarily needs to support the model inside the wind tunnel, which is in contradiction to the actual condition which is a free-free configuration.

There have been some attempts to identify the best way to support the model and in this respect it is relevant to point out here that the buffet response is generally concentrated in the first three free-free modes of the model and the responses in higher modes are either marginal or negligible. With this in mind the model is normally supported on springs at the nodal points corresponding to the first free-free mode and the stiffness of the springs is so adjusted that it has minimum interference with the higher model modes. Ideally, the springs should offer only translational resistance at the node points but a practical spring configuration also offers significant resistance to rotational motion at the node points. Also, if the springs are too flexible, there are likely to be large static deflections under the self-weight and the steady aerodynamic loads, resulting in significant changes in the preset angles of attack. Therefore, a compromise has to be reached in arriving at the appropriate values for the spring stiffness and this has to be done by trial and error because no guidelines exist as yet for choosing the most suitable value of the spring stiffness for a given model configuration.

The present study is an examination of the effect of an elastic support system, consisting of a cantilevered rod and a pair of springs, on the free vibration characteristics of a typical spacecraft model with a view to investigate the dynamic modal coupling between the model and the elastic support system. The simple elementary beam formulation is used, and the problem is solved exactly to yield the results for the frequency and the generalized modal mass as a function of the support elasticity. In particular, the study is aimed at bringing out the effect of rotational spring stiffnesses on the frequencies and the generalized modal masses of the spacecraft and also their interaction with the translational stiffnesses. The study is also aimed at bringing out the influence of a shift in the support point location, away from the nodal points. For the purpose of analysis a uniform slender beam is taken to represent the spacecraft model.

2. FORMULATION AND SOLUTION

Figure 1 shows the configuration of the model and support system. It consists of the model connected to another uniform beam, which is clamped at one end and free at the other end, by two translational springs and two rotational springs. The cantilevered beam acts as a support rod inside the wind tunnel and is also known as the sting rod. Points 1 and 2 are the nodal points corresponding to the first free-free mode of a uniform beam. The governing differential equation of motion, in each of the five beam segments, based on the elementary theory of beams can be given as, (a list of nomenclature is given in the Appendix)

$$E_j I_j \, \partial^4 u_j / \partial z_j^4 + \rho_j A_j \, \partial^2 u_j / \partial t^2 = 0, \tag{1}$$

where $j = 1, 2, 3, 4, 5$ denote each of the five segments. For harmonic vibration one can assume the solution in general form as

$$u_j(z, t) = u_j(z) \sin \omega t. \tag{2}$$

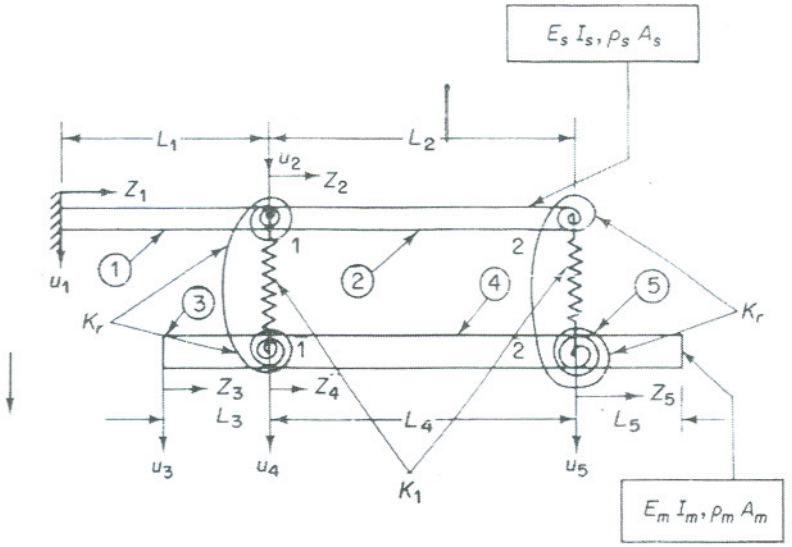

Figure 1. Elastically interconnected beams: geometry and co-ordinate systems.

Substituting the solution (2) into the governing equation (1) and suitably non-dimensionalizing it gives

$$\partial^4 \bar{u}_j / \partial \bar{z}_j^4 - \lambda_j^4 \bar{u}_j = 0, \tag{3}$$

where $\bar{z}_j$ is the dimensionless length co-ordinate in each of the beam segment, $\bar{u}_j$ is the dimensionless displacement in each of the five beam segments and λ_j is the corresponding frequency parameter, which is related to λ, the dimensionless frequency parameter, by

$$\lambda_j^4 = \{(\rho_0 A_0 / \rho_j A_j)(L_0^4 / L_j^4)(E_j I_j / E_0 I_0)\}\lambda^4, \tag{4}$$

where the quantities with suffix 0 correspond to a reference beam and the quantities with suffix j correspond to the jth beam segment. In operator form equation (3) can be rewritten as

$$(P_j^4 - \lambda_j^4)\bar{u}_j = 0. \tag{5}$$

The general solution of equation (5) is given by

$$\bar{u}_j = A_j \cosh \lambda_j \bar{z}_j + B_j \sinh \lambda_j \bar{z}_j + C_j \cos \lambda_j \bar{z}_j + D_j \sin \lambda_j \bar{z}_j, \tag{6}$$

where A_j, B_j, C_j and D_j are the arbitrary constants corresponding to the jth beam segment.

Equation (6) represents the five displacement functions with a total of 20 unknown constants which are to be determined by applying the boundary conditions and the junction conditions.

2.1. BOUNDARY CONDITIONS

The general solution given by equation (6) needs to satisfy the cantilever boundary conditions on the support rod and free-free boundary conditions at the two ends of the model. Therefore, one has the following six boundary conditions.

$$\bar{u}_1(\bar{z}_1 = 0) = (\partial \bar{u}_1 / \partial \bar{z}_1)(\bar{z}_1 = 0) = 0, \qquad (\partial^2 \bar{u}_3 / \partial z_3^2)(\bar{z}_3 = 0) = (\partial^3 \bar{u}_3 / \partial \bar{z}_3^3)(\bar{z}_3 = 0) = 0, \tag{7, 8}$$

$$(\partial^2 \bar{u}_5 / \partial \bar{z}_5^2)(\bar{z}_5 = 0) = (\partial^3 \bar{u}_5 / \partial \bar{z}_5^3)(\bar{z}_5 = 0) = 0. \tag{9}$$

2.2. JUNCTION CONDITIONS

It can be seen from Figure 1 that the support rod and the model are connected to each other at points 1 and 2 through elastic springs and therefore one needs to satisfy the necessary twelve conditions at these points. These conditions include the displacement and slope continuity equations and the shear force and bending moment balance equations. These conditions can be written in two parts as follows.

2.2.1. *Displacement and slope continuity conditions*

The continuity of displacement and slope at the junction of segment 1 and 2 are given as

$$\bar{u}_1(\bar{z}_1 = 1) = \bar{u}_2(\bar{z}_2 = 0), \qquad (d\bar{u}_1/\partial\bar{z}_1)(\bar{z}_1 = 1) = (\partial\bar{u}_2/\partial\bar{z}_2)(\bar{z}_2 = 0). \tag{10, 11}$$

Similarly, there are four more conditions on the displacements and slopes at the junctions of segments 3 and 4 and of segments 4 and 5.

2.2.2. *Shear force and bending moment balance*

From equilibrium considerations it is necessary that all the forces and moments should balance each other at a junction. The conditions on shear force and bending moment at the junction of segment 1 and 2 are as follows:

$$-E_1 I_1(\partial^3\bar{u}_1\partial\bar{z}_1^3)(1) + K_1\{\bar{u}_1(1) - \bar{u}_3(1)\} + E_2 I_2(\partial^3\bar{u}_2/\partial\bar{z}_2^3)(0) = 0, \tag{12}$$

$$-E_1 I_1(\partial^2\bar{u}_1/\partial\bar{z}_1^2)(1) - K_r\{\bar{u}_1'(1) - \bar{u}_3'(1)\} + E_2 I_2(\partial^2\bar{u}_2/\partial\bar{z}_2^2)(0) = 0. \tag{13}$$

Similarly, there are six more conditions on the forces and moments at the other three junction points. Thus there are a total of 20 conditions for 20 unknowns of the general solution given by equation (6).

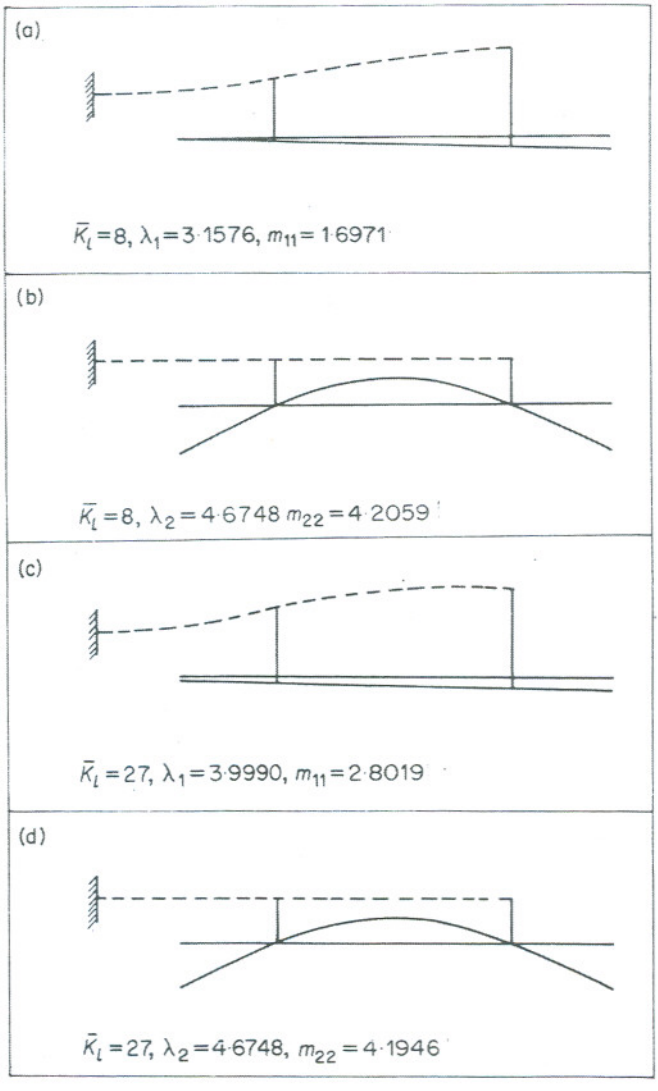

Figure 2. Normalized mode shapes for two values of the linear stiffness parameter, $\bar{K}_t$, and zero rotational stiffness. (a) and (c) predominantly first support rod modes: (b) and (d) predominantly first model modes. ——, model; - - -, support rod mode.

Substitution of the general solution (6) into the equations (7)–(13) results in a set of 20 homogeneous simultaneous transcendental equations and for a non-trivial solution of this system of equations, the determinant of the coefficients matrix is set to zero.

3. NUMERICAL RESULTS FOR VARIOUS SUPPORT STIFFNESSES

Figures 2–8 present the numerical results for the frequencies, the mode shapes and the generalized modal mass values of the coupled elastic support-model system for various values of the linear spring stiffness parameter, $\bar{K}_l$ and the rotational spring stiffness parameter, $\bar{K}_r$.

It may be recalled here that the model is connected to the support system at the points corresponding to the nodes of the first free-free mode of the model and therefore it is expected that in the absence of rotational stiffness the translational stiffness should not have any effect on the first model mode. In fact, Figure 2(b) shows that the normalized mode shape of the model, shown by the solid line (for the case of $\bar{K}_l = 8$ and $\bar{K}_r = 0$), is identical to the first free-free model bending mode. (Here it may be relevant to point out that for a free-free model with no support, the value of λ_2 is 4·6748 and m_{22} is 4·2059.) It can also be seen from Figure 2(d) that increase in the linear spring stiffness from 8 to 27 has no influence on the model mode. It can also be seen from Figures 2(a) and 2(b) that for both $\bar{K}_l = 8$ and 27, there is very little model deflection in the predominantly first support rod mode and this is also of the rigid body type. The differences between the first support rod mode shapes for $\bar{K}_l = 8$ and 27 come primarily from the increased deflection and curvature in the support rod itself. It is also relevant to mention here that

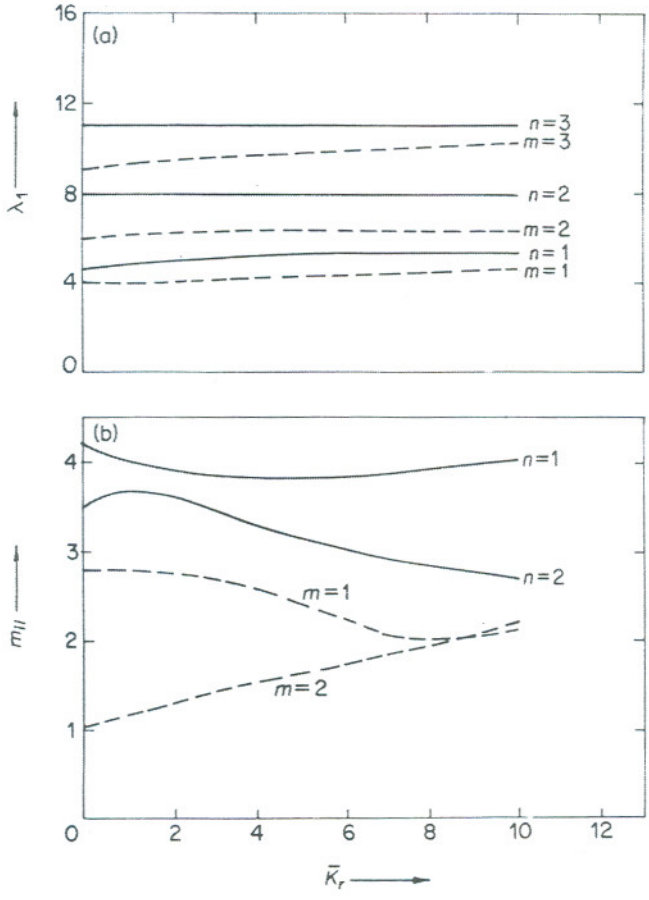

Figure 3. Variation of (a) freqeuncy parameter, λ_i, and (b) generalized mass parameter m_{ii}, versus the rotational stiffness parameter, $\bar{K}_r$, for $\bar{K}_l = 27$. ——, model; – – –, support rod.

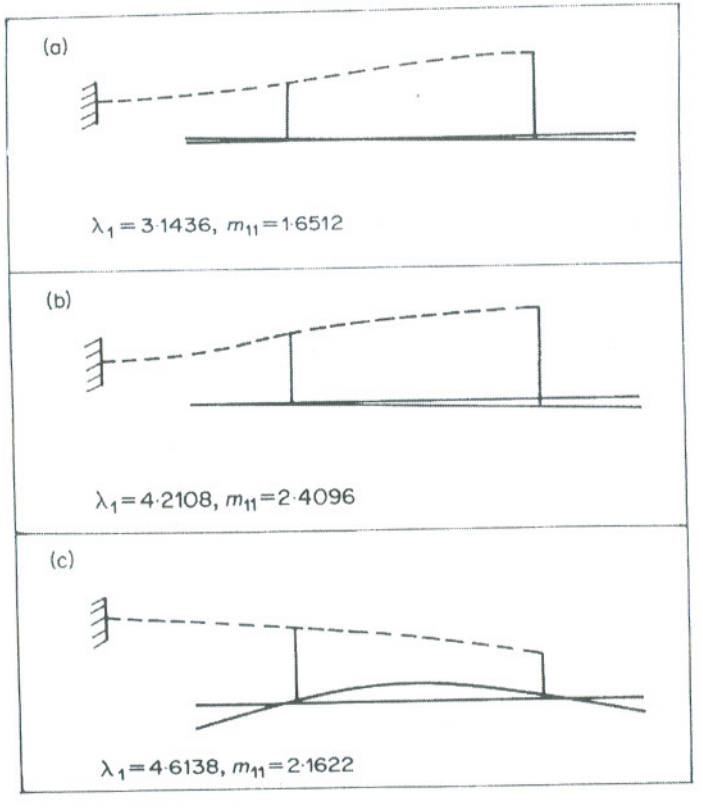

Figure 4. Normalized mode shapes for the predominantly first support rod mode for (a) $\bar{K}_l = 0$ and $\bar{K}_r = 5$, (b) $\bar{K}_l = 27$ and $\bar{K}_r = 5$ and (c) $\bar{K}_l = 27$ and $\bar{K}_r = 10$. ——, model; - - -, support rod.

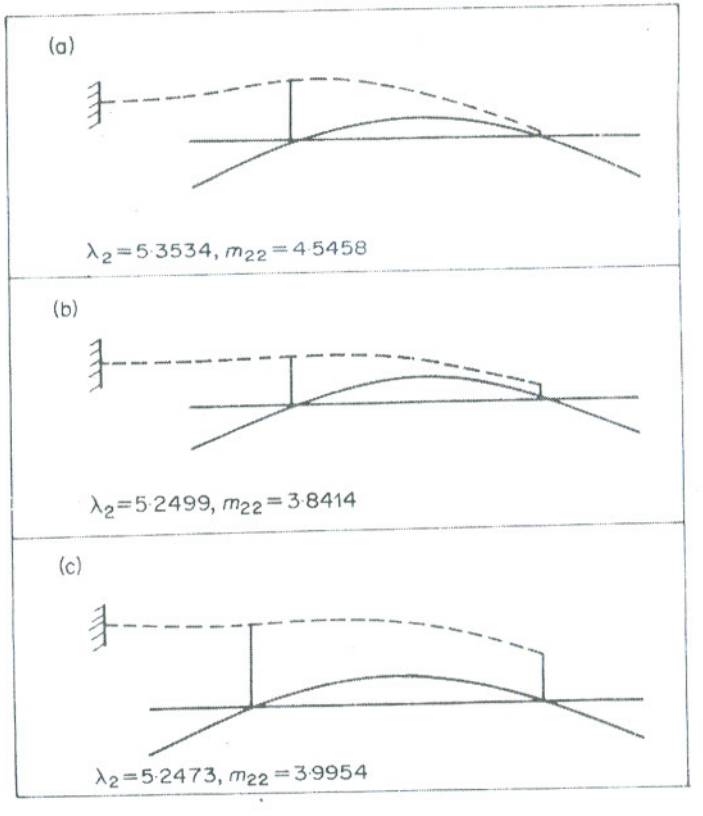

Figure 5. Normalized mode shapes for the predominantly first model mode for (a) $\bar{K}_l = 0$ and $\bar{K}_r = 5$, (b) $\bar{K}_l = 27$ and $\bar{K}_r = 5$ and (c) $\bar{K}_l = 27$ and $\bar{K}_r = 10$. ——, model; - - -, support rod.

the higher model modes (i.e., second, third, etc.) are negligibly influenced for the cases of both $\bar{K}_l = 8$ and $\bar{K}_l = 27$. This is probably because of the fact that the higher modes contain a larger amount of strain energy and therefore the contribution to it arising from the springs is comparatively negligible.

Figure 3 shows the effect of rotational spring stiffness parameter $\bar{K}_r$ for the case of $\bar{K}_l = 27$ in terms of the variation of the frequencies and the generalized modal masses. Here m denotes the number of the predominantly support rod mode and n denotes the predominantly model mode. It can be seen that even though the frequency of only the first model mode is noticeably altered with $\bar{K}_r$ increasing from 0 to 12, the total generalized masses in both the first and the second model modes (denoted by $n = 1$ and 2) are significantly affected. This indicates that the model mode shapes for these two cases are altered significantly and, therefore, it is now appropriate to examine the individual mode shapes in greater detail.

Figure 4 shows the influence of $\bar{K}_r$ on the first support rod mode and it can be seen that for $\bar{K}_l = 0$ and $\bar{K}_r = 5$, the model deflection in this mode is negligible. When $\bar{K}_l$ is raised to 27, both the frequency and the generalized mass values are increased substantially. However, when $\bar{K}_r$ is increased to 10, while keeping the $\bar{K}_l$ constant at 27, the frequency of the predominantly first support rod mode increases while the generalized mass for the same mode decreases. This can be attributed to the fact that the support rod deflection pattern (indicated by the broken line) has changed and it is also interesting to note that the model deflection pattern in this mode closely resembles the predominantly first model mode excepting for the actual deflection levels. This closeness is also manifest in the value of the frequency for this mode which is 4·6168 and is quite close to the free-free value of 4·6786.

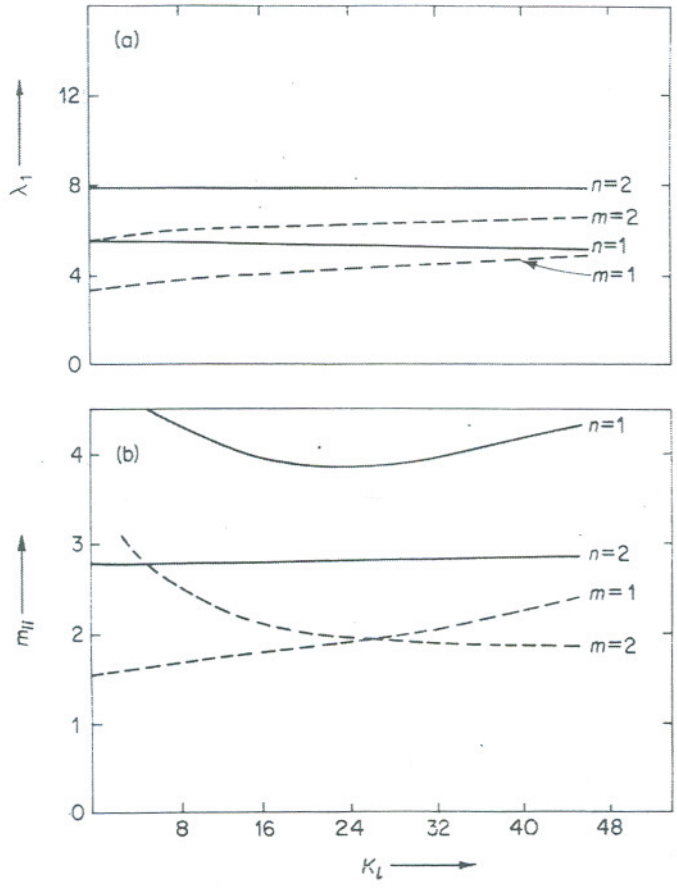

Figure 6. Variation of (a) the frequency parameter, λ_i and (b) the generalized mass parameter, m_{ii}, versus $\bar{K}_l$ for $\bar{K}_r = 8$. ——, model; - - -, support rod.

Figure 5 shows the variation of the predominantly first model mode shape for different values of $\bar{K}_l$ and $\bar{K}_r$. It can be seen from Figure 5(a) that a rotational restraint only of $\bar{K}_r = 5$ produces a significant amount of curvature in the support rod and also noticeably shifts the nodal points away from the support location. This is because, in the absence of any translational restraint, the support rod is constrained to follow the slope of the model at the junctions. As a result of this, the motion of the support rod gets strongly coupled to the motion of the model. Figure 5(b) shows that as $\bar{K}_l$ is increased from 0 to 27, the deflection levels in the support rod come down considerably, thereby indicating that the linear springs tend to reduce the curvatures. This is manifest as a reduction in both the frequency and the generalized mass for $\bar{K}_l = 27$, $\bar{K}_r = 5$. However, when $\bar{K}_r$ is increased from 5 to 10 for the same value of $\bar{K}_l = 27$, it is found that λ_2 remains practically unchanged while m_{22} increases slightly. A closer examination of Figure 5(c) shows that the increased rotational stiffness causes changes only in the support rod curvatures leaving the model mode reasonably unaffected. In all the Figures 5(a), (b) and (c) it is found that a relatively small rotational stiffness of $\bar{K}_r = 5$ introduces a very strong coupling between the model and the support system and therefore it now becomes necessary to study the effect of rotational restraint in greater detail.

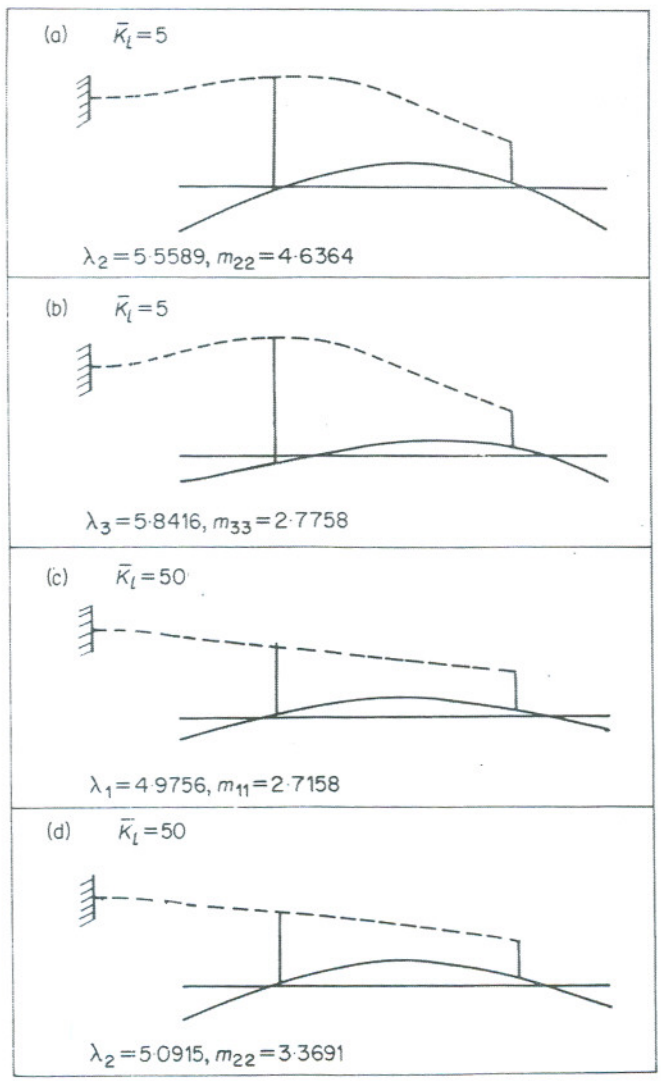

Figure 7. Normalized mode shape for two values of $\bar{K}_l$, 5 and 50, and for $\bar{K}_r = 8$; (b) and (c) predominantly support rod modes; (a) and (d), predominantly model modes. ——, model; – – –, support rod.

Figure 6 shows the variation of λ_i and m_{ii} with $\bar{K}_l$ for $\bar{K}_r = 8$. It can be seen that for very low values of $\bar{K}_l$, the predominantly first model mode frequency almost coincides with predominantly second support rod mode frequency. However, as $\bar{K}_l$ increases, these two separate and λ_2 reduces and merges with the predominantly first support rod mode for $\bar{K}_l = 50$. This indicates that there is a gradual change in the support rod mode shape in the predominantly first model mode from a typical second cantilever mode form to a typical first cantilever mode. On the other hand, the generalized mass for the same mode ($n = 1$) has a minimum around $\bar{K}_l = 25$ and increases for both low as well as high values of $\bar{K}_l$. This increase, as will be seen shortly, is because of increased contribution from the support rod for both the limits of $\bar{K}_l = 5$ and $\bar{K}_l = 50$. Figure 7(a) shows a comparison of the predominantly second support rod mode and the predominantly first model mode and it can be seen that there is a significant amount of interaction between the model and the support rod in both the modes. In fact it becomes almost impossible to differentiate between the two modes and only the model deformation decides which is the predominantly model mode and which is the predominantly support rod mode. Figure 7(b) shows the other limit of this interaction as signified by $\bar{K}_l = 50$ where the predominantly first model mode approaches the predominantly first support rod mode. Here also it is seen that there is substantial deflection of the support rod in the predominantly model mode and only the model deflection shape and levels decide which is the model mode and which is the support mode.

All the results discussed till now have presented the variation of the total generalized modal mass only, which, as has been seen, is a combination of the generalized mass of

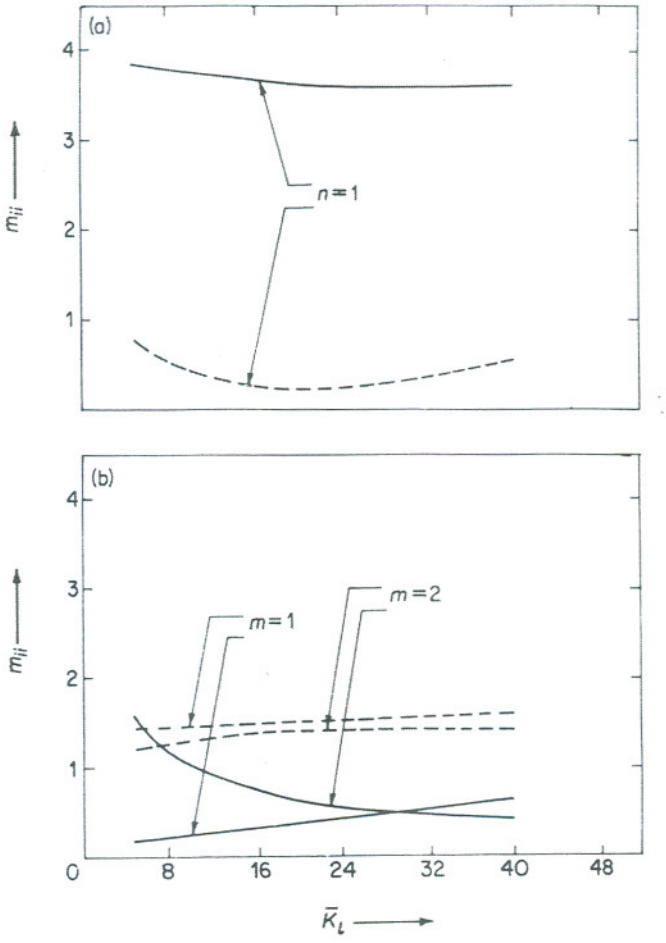

Figure 8. Variation of the generalized mass components for (a) predominantly model modes and (b) predominantly support rod modes versus $\bar{K}_l$ for $\bar{K}_r = 8$. ——, model - - -, support rod.

the model and of the support rod. Many times it is very useful to know the individual values of the generalized masses which not only give a fairly good idea of the energy content in the individual components but also decide which segment is predominating, if one uses a common base for non-dimensionalization. Figure 8 shows the generalized mass variation in terms of its components, for the predominantly first model mode and the predominantly first and second support rod modes. It can be seen from Figure 8(a) that for low values of $\bar{K}_l$ the generalized mass in the model drops slightly and then remains practically constant for higher values of $\bar{K}_l$. The generalized mass in the support rod has a minima around $\bar{K}_l = 24$ indicating that for both low and high values of $\bar{K}_l$ there is an increased support rod deflection. In fact this explains the minimum also observed in the total generalized mass in Figure 6(b). Figure 8(b) shows that the content of generalized mass in the model is very low in the predominantly first support rod mode and high in the predominantly second support rod mode for low values of $\bar{K}_l$. This is understandaable as the model first mode is coupled to the support rod second mode for low values of $\bar{K}_l$. Similar coupling of the model mode for high values of $\bar{K}_l$ is manifest as an increase in the model generalized mass in the first support rod mode.

4. EFFECT OF THE SUPPORT ROD STIFFNESS AND INERTIA

For results presented in Figures 2–8 the support rod configuration has been considered as constant with the support rod stiffness parameter $(EI)_s/(EI)_m = 0{\cdot}8$ and the support rod inertia parameter $(\rho A)_s/\rho A)_m = 0{\cdot}5$. However, it is important to investigate also the effect of variation in these parameters on the free vibration characteristics of the coupled

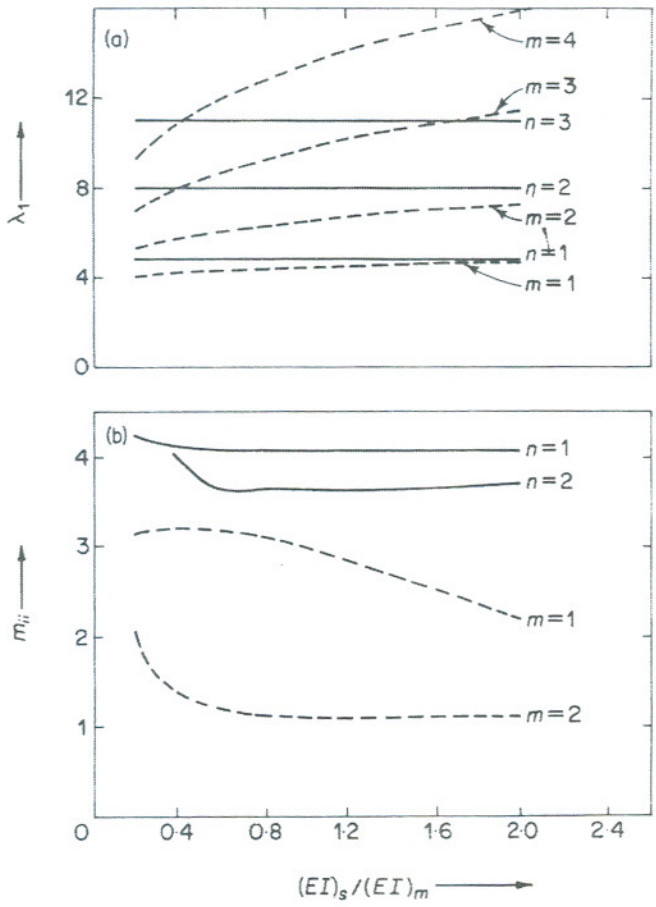

Figure 9. Variation of (a) λ_i and (b) m_{ii} versus the support stiffness parameter, $(EI)_s/(EI)_m$, for $\bar{K}_l = 45$ and $\bar{K}_r = 0{\cdot}5$. ——, model; – – –, support rod.

system and to see whether or not there is an optimum value for these parameters which ensures minimum support interference.

Figure 9 shows the variation of the frequency parameter, λ_i, and the generalized mass parameter, m_{ii}, with the support stiffness parameter for a high linear stiffness ($\bar{K}_l = 45$) and negligible rotational stiffness ($\bar{K}_r = 0{\cdot}5$). It can be seen that as $(EI)_s$ increases, all the support rod mode frequencies denoted by various values of m increase. However, there is no influence of this increase in the support rod stiffness on any of the model modes mainly because there is no rotational restraint present. Therefore, one might come to a slightly erroneous conclusion that the support rod stiffness variations are not important if there is no rotational restraint present. Figure 9(a) also reveals the fact that, as $(EI)_s$ increases, the support rod frequencies come close to or cross over the first three model frequencies. For example, at the value of $(EI)_s/(EI)_m = 0{\cdot}4$ the third and fourth support rod frequencies are almost the same as the second and third model frequencies respectively. This closeness of two modes adversely affects the overall response of the system because there will be a significant energy content in the support rod when the model is being excited. Therefore, even though the variations in the support rod stiffness do not directly influence the model modes, the closeness of support rod modes has to be avoided in deciding the support rod stiffness.

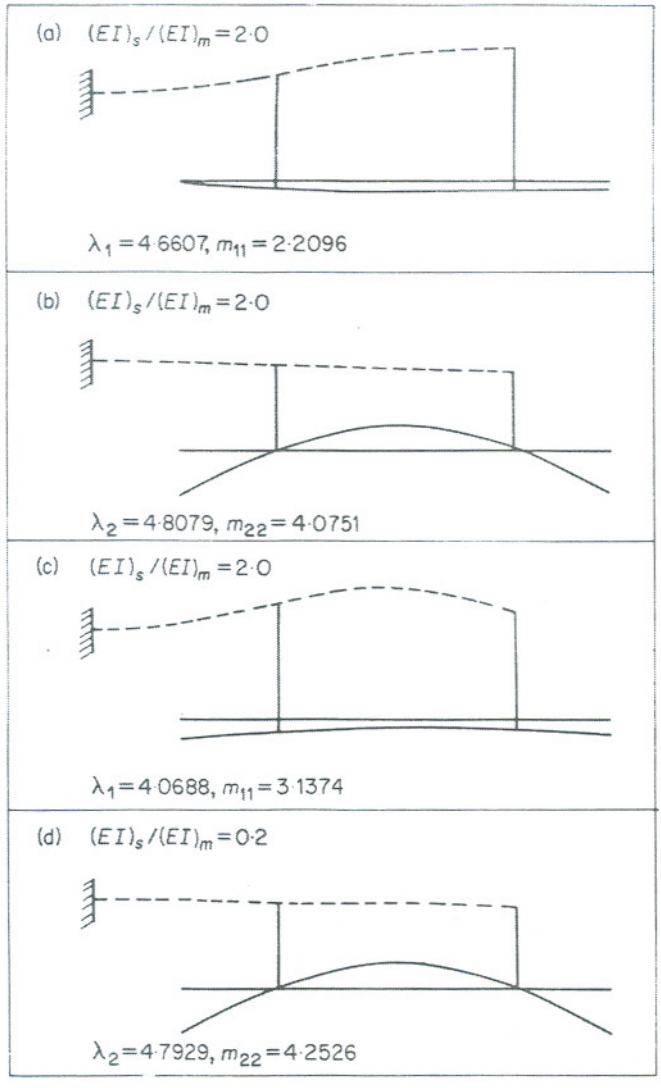

Figure 10. Normalized mode shapes for $(EI)_s/(EI)_m = 2{\cdot}0$ and $0{\cdot}2$; (a) and (c) predominantly support rod mode; (b) and (d), predominantly model mode. ——, model – – –, support rod.

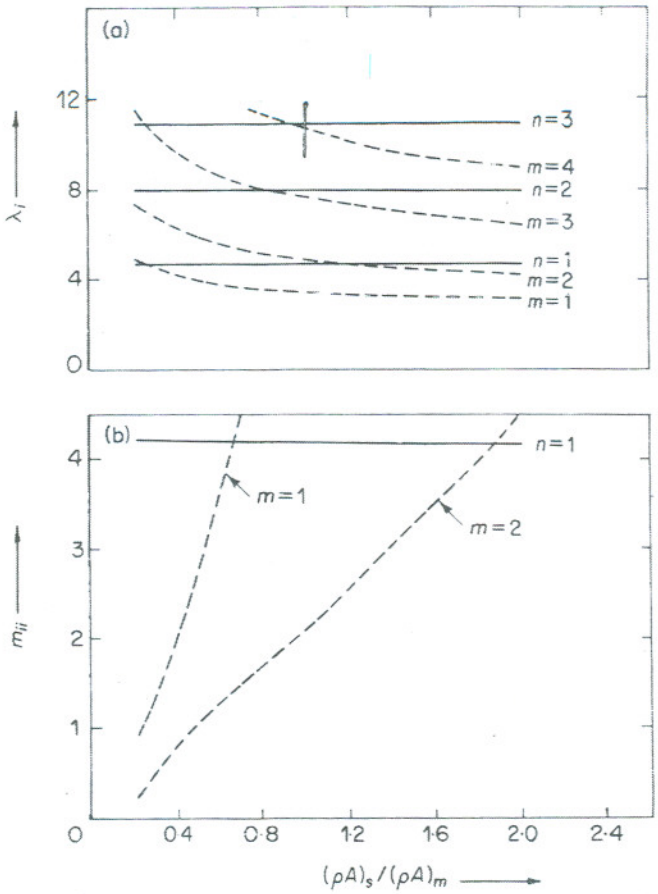

Figure 11. Variation of (a) λ_i and (b) m_{ii} versus the support rod inertia parameter, $(\rho A)_s/(\rho A)_m$ for $\bar{K}_l = 27$ and $\bar{K}_r = 0{\cdot}01$. ——, model; – – –, support rod.

Figure 10 shows the normalized mode shapes for two cases of $(EI)_s/(EI)_m = 0{\cdot}2$ and $(EI)_s/(EI)_m = 2{\cdot}0$ for $\bar{K}_l = 45$ and $\bar{K}_r = 0{\cdot}5$. It can be seen that the predominantly model mode is more or less the same as the pure free-free model mode. It can also be seen that model deflections are only marginal in the predominantly support rod mode.

The effect of increasing the support rod inertia is the reverse of increasing the support rod stiffness, as shown in Figure 11. Here the support rod frequencies decrease with increasing inertia but, similarly as in the case of increasing $(EI)_s$, the support rod frequencies again cross over the model frequencies as the inertia is increased but the model modes remain unaffected. In fact, from both the Figures 9 and 11 one can arrive at fairly good estimates for the support rod stiffness parameter and the support rod inertia parameter which will ensure the maximum separation between the predominantly model mode frequencies and the predominantly support rod mode frequencies. Figure 12(a) and (b) show that for both very low support rod inertia $\{(\rho A)_s/(\rho A)_m = 0{\cdot}2\}$ and very high support rod inertia, $\{(\rho A)_s/(\rho A)_m = 1{\cdot}0\}$, the mode shapes are practically the same.

Thus, the results presented in Figures 9–12 clearly show that, even though the support rod configuration does not influence the model modes directly if the rotational restraint is absent, the choice of the support rod stiffness and inertia parameters should be dictated by the considerations of maximization of the frequency separation.

5. EFFECT OF SHIFT IN THE MODEL SUPPORT POINTS LOCATION

It was mentioned earlier that in order to minimize the support interference with the first free-free model mode, the model is supported at the node points corresponding to

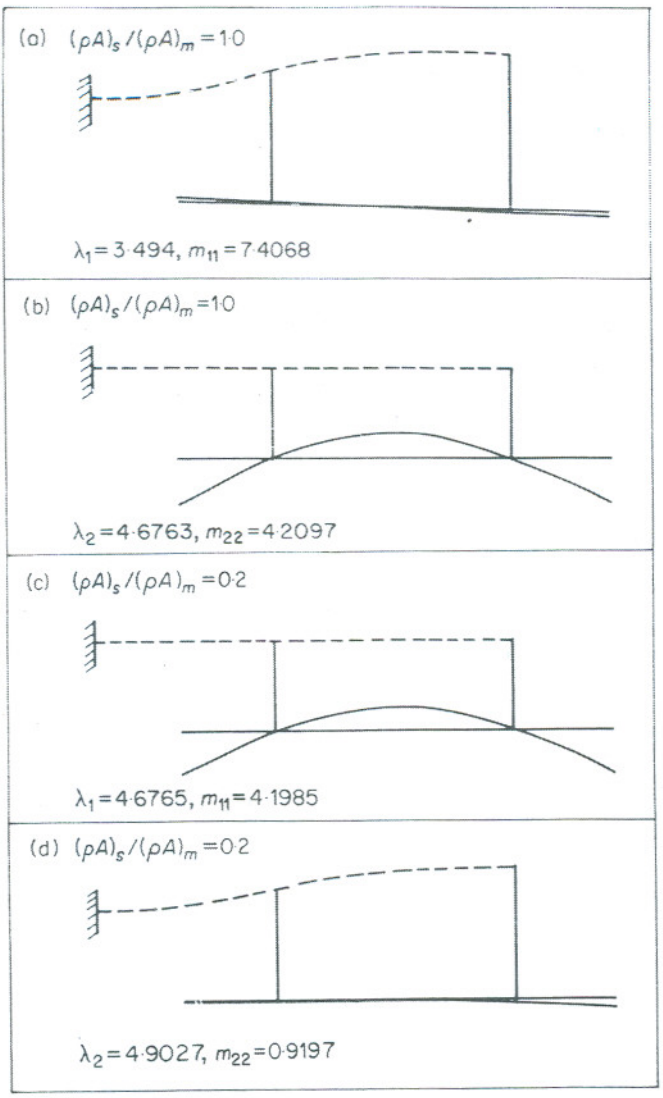

Figure 12. Normalized mode shapes for $(\rho A)_s/(\rho A)_m = 1{\cdot}0$ and $0{\cdot}2$; (a) and (d) predominantly support rod modes; (b) and (c) predominantly model modes. ——, model; - - -, support rod.

this mode. However, in practice, there may be certain difficulties in achieving this and it may become necessary to support the model at points away from the nodes. This shift is likely to influence the overall response of the coupled system and it is very useful to quantify the effect of such a shift on the total response of the coupled system.

Figure 13 shows the variation of the generalized mass in the predominantly first model mode with the support shift parameter, Δx for two cases of $\bar{K}_l = 5$ and $\bar{K}_l = 40$. It can be seen that the generalized mass is significantly affected for both $\bar{K}_l = 5$ and $\bar{K}_l = 40$ but there is a slight difference between the two. It may be recalled that the total generalized mass is a combination of the generalized mass contribution from the support rod and from the model. It is seen that for $\bar{K}_l = 5$ the support rod has no generalized mass contribution and the effect of the support shift is evident in the model mode shape only. However, for $\bar{K}_l = 40$ the support rod deforms significantly as indicated by an increased mass contribution coming from the support rod. This trend is also manifest in Figure 14 where the mode shapes for both $\bar{K}_l = 5$ and $\bar{K}_l = 40$ are shown for both $\Delta x = -0{\cdot}08$ and $\Delta x = 0{\cdot}06$. It can be seen that for $\bar{K}_l = 5$ the support rod does not deform at all and that the effect of the support shift is felt fully in the model mode shape only. This perhaps can be attributed to the fact that the support rod is much stiffer than the linear springs and therefore does not deform for low values of $\bar{K}_l$. For the case of $\bar{K}_l = 40$, it can be

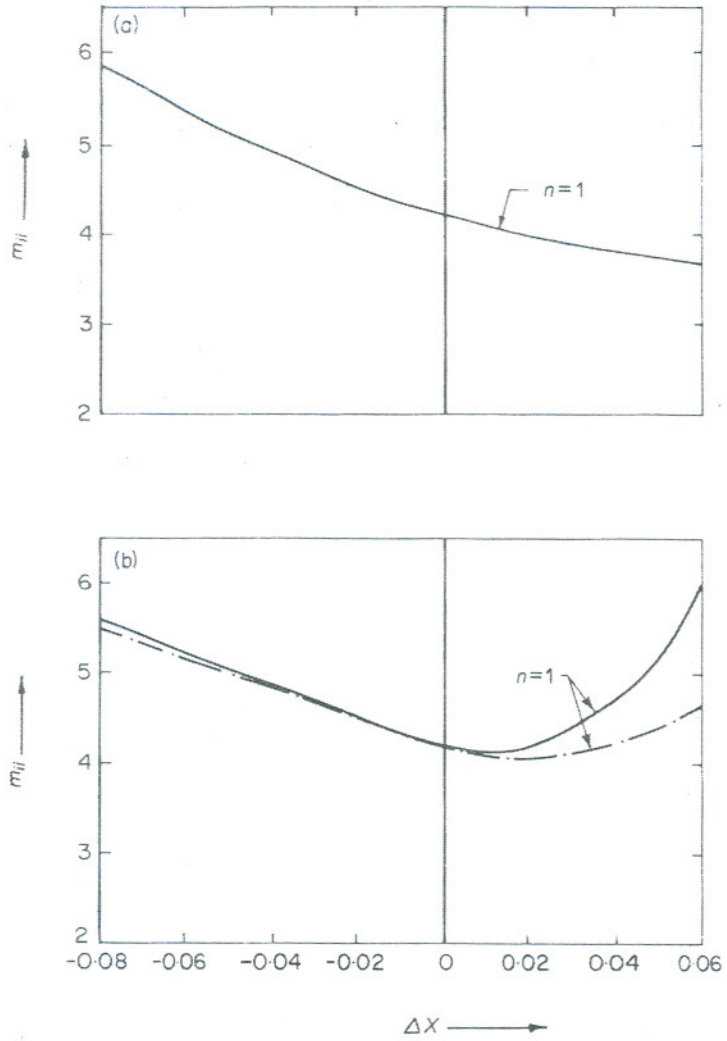

Figure 13. Variation of the generalized mass parameter m_{ii} versus the support offset parameter Δx for predominantly first mode for (a) $\bar{K}_l = 5$ and (b) $\bar{K}_l 40$. ——, model; - - -, support rod mode.

seen that as one increases the offset parameter, Δx, there is a significant deformation of the support rod along with the model. This means that for $\bar{K}_l = 40$ the support rod stiffness becomes comparable to $\bar{K}_l$ and this results in the deformations of the support rod. This can explain the observation that for both low spring stiffnesses (lower than the support rod stiffness) and high spring stiffnesses (comparable to or higher than the support rod stiffness), the shift in the model support points has almost equal effects on the model mode shape. However, there is a need to study the support offset influence in conjunction with the support rod stiffness in greater detail to arrive at some specific conclusions.

6. CONCLUSIONS

A study of the problem of vibration of a uniform beam on two intermediate elastic supports has been presented. The uniform beam represents a launch vehicle structural model designed for aeroelastic buffet testing. Numerical results for the frequencies, mode shapes and the generalized modal masses have been obtained for the various values of the dimensionless linear spring stiffness parameter, rotational-spring stiffness parameter, the support rod stiffness parameter, the support rod inertia parameter and the support offset parameter. The results show that when the model is supported on the node points corresponding to the first pure free-free beam mode, its first mode vibration characteristics

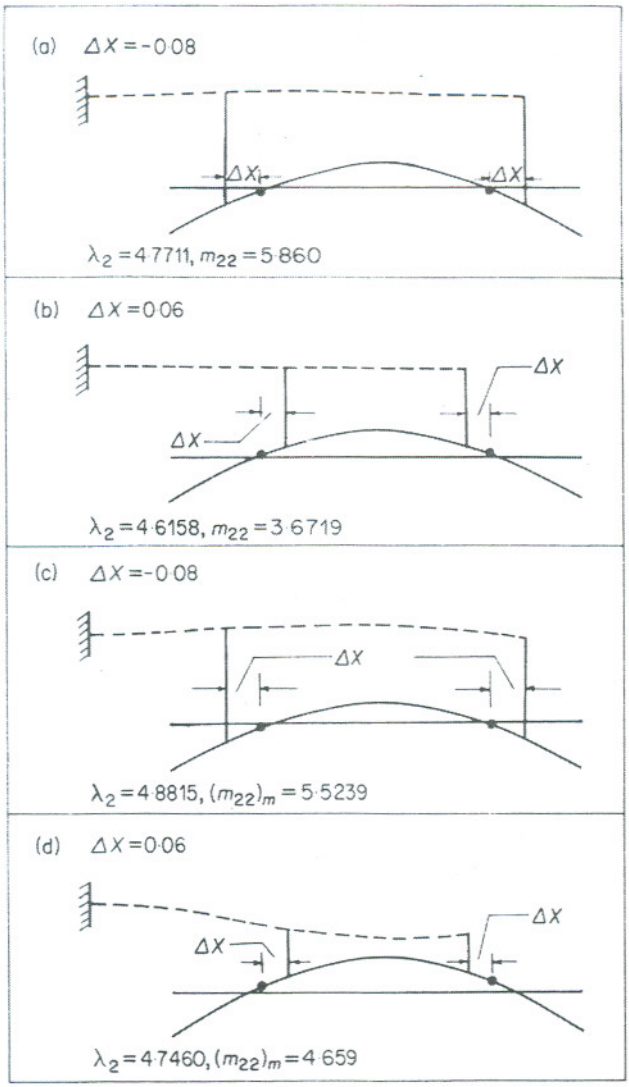

Figure 14. Normalized mode shapes for the predominantly model mode for two values of the support offset parameter, $\Delta x = -0{\cdot}08, 0{\cdot}06$. (a) and (b) $\bar{K}_l = 5$; (c) and (d) $\bar{K}_l = 40$. ——, model; - - -, support rod.

remain practically unaltered if there is no rotational restraint present. However, in the presence of rotational restraint, there is a significant amount of interaction between the model and the support system and therefore as far as possible the rotational restraint should be minimized. The results also show that, although the support rod configuration (i.e., its stiffness and inertia values) affects only the support rod modes, it is necessary to avoid the various cross-overs of support rod frequencies and to ensure that there is a sufficient separation of frequencies in order to avoid simultaneous excitation of the support rod modes. Finally, the influence of the offset in the support rod location has also been investigated and it has been shown that although the frequency of the model is only marginally affected the generalized mass is altered significantly.

REFERENCES

1. P. W. HANSON and G. W. JONES 1963 *Presented at the Symposium Aeroelastic and Dynamic Modelling Technology, Dayton, Ohio*, 23-25 *September*. On the use of dynamic models for studying launch buffet and ground-wind loads.
2. W. H. LIN and M. T. CHEN 1983 24*th AIAA/ASME/ASCE/AHS SDM Conference, Paper No.* 83-0928. Buffeting of a slender circular beam in axial turbulent flows.

3. R. V. DOGGET JR. and P. W. HANSON 1963 *NASA TN D*-2022. An aeroelastic model approach for the prediction of buffet bending loads on launch vehicles.
4. P. W. HANSON and R. V. DOGGET JR. 1965 *NASA TN D*-2713. Aerodynamic damping and buffet response of an aeroelastic model of the Saturn I Block II launch vehicle.
5. J. T. UCHIYAMA and F. W. PETERS 1968 *The Shock and Vibration Bulletin* **37**, 121-136. Buffet response measurements of a seven percent aeroelastically scaled model of various TITAN III configurations.

APPENDIX: NOMENCLATURE

A_j	unknown constant in equation (6) and cross-sectional area of the jth segment
B_j, C_j, D_j	unknown constants in equation (6)
E_jI_j	beam segment bending stiffness
E_0I_0	reference beam bending stiffness
E_sI_s	support rod bending stiffness
E_mI_m	model bending stiffness
K_l	linear spring stiffness
K_r	rotational spring stiffness
$\bar{K}_l$	$(=K_lL_0^3/E_0I_0)$, dimensionless value of K_l
$\bar{K}_r$	$(=K_rL_0/E_0I_0)$, dimensionless value of K_r
L_j	jth beam segment length
L_0	reference length
P_j	$(=\partial/\partial\bar{z}_j)$, the dimensionless differential operator
m	index number of predominantly support rod mode
m_{ii}	$(=\sum\int\bar{u}_i^2\,dm)$, generalized mass of ith mode
n	index number of predominantly model mode
u	displacement in x-direction
x, y, z	Cartesian co-ordinate system
$\bar{u}$	dimensionless value of u
$\bar{u}_j$	dimensionless displacement in segments
$\bar{z}_j$	$(=z_j/L_j)$, dimensionless z-co-ordinate in the jth beam segment
ρ_0	reference mass density
ρ_j	mass density of jth beam segment
λ	$(=\rho_0\omega^2L_0^4A_0/E_0I_0)$, dimensionless frequency parameter
λ_i	value of frequency parameter, λ, for ith mode
λ_j	$(=\rho_j\omega^2L_j^4A_j/E_jI_j)$, dimensionless frequency parameter with respect to the jth beam segment
Δx	support point offset parameter
$'$	superscript denotes differentiation with respect to $\bar{z}_j$